Atmos. Meas. Tech. Discuss., 8, 10897–10935, 2015
www.atmos-meas-tech-discuss.net/8/10897/2015/
doi:10.5194/amtd-8-10897-2015

Atmospheric Measurement Techniques Discussions
Open Access
EGU

Validation of TANSO-FTS/GOSAT XCO_2 and XCH_4 glint mode retrievals using TCCON data from near-ocean sites

M. Zhou[1,2,3], B. Dils[2], P. Wang[1], R. G. Detmers[4], Y. Yoshida[5], C. W. O'Dell[6], D. G. Feist[7], V. Velazco[8], M. Schneider[9], and M. De Mazière[2]

[1]Key Laboratory of Middle Atmosphere and Global Environment Observation, Institute of Atmospheric Physics, Chinese Academy of Sciences, Beijing, China
[2]Belgian Institute for Space Aeronomy, Brussels, Belgium
[3]University of Chinese Academy of Sciences, Beijing, China
[4]SRON Netherlands Institute for Space Research, Utrecht, the Netherlands
[5]National Institute for Environmental Studies, Tsukuba, Japan
[6]Colorado State University, Fort Collins, CO, USA
[7]Max Planck Institute for Biogeochemistry, Jena, Germany
[8]Centre for Atmospheric Chemistry, University of Wollongong, Wollongong, Australia
[9]Institute of Meteorology and Climate Research (IMK-ASF), Karlsruhe Institute of Technology, Karlsruhe, Germany

Received: 25 September 2015 – Accepted: 8 October 2015 – Published: 26 October 2015

Correspondence to: M. Zhou (zhouminqiang@mail.iap.ac.cn)
and B. Dils (bart.dils@aeronomie.be)

Published by Copernicus Publications on behalf of the European Geosciences Union.

Abstract

Thermal And Near infrared Sensor for carbon Observations Fourier Transform Spectrometer (TANSO-FTS) on board The Greenhouse gases Observing SATellite (GOSAT) applies the normal nadir mode above the land ("land data") and sun glint mode over the ocean ("ocean data") to provide global distributions of column-averaged dry-air mole fractions of CO_2 and CH_4, or XCO_2 and XCH_4. Several algorithms have been developed to obtain highly accurate greenhouse gas concentrations from TANSO-FTS/GOSAT spectra. So far, all the retrieval algorithms have been validated with the measurements from ground-based Fourier transform spectrometers from the Total Carbon Column Observing Network (TCCON), but limited to the land data. In this paper, the ocean data of the SRPR, SRFP (the proxy and full-physics versions 2.3.5 of SRON/KIT's RemoTeC algorithm), NIES (National Institute for Environmental Studies operational algorithm version 02.21) and ACOS (NASA's Atmospheric CO_2 Observations from Space version 3.5) are compared with FTIR measurements from five TCCON sites and near-by GOSAT land data.

For XCO_2, both land and ocean data of NIES, SRFP and ACOS show good agreement with TCCON measurements. Averaged over all TCCON sites, the relative biases of ocean data and land data are 0.33 and 0.13 % for NIES, −0.03 and −0.04 % for SRFP, −0.06 and 0.03 % for ACOS, respectively. The relative scatter ranges between 0.31 and 0.49 %. For XCH_4, the relative bias of ocean data is even less than that of the land data for the NIES (−0.02 vs. 0.35 %), SRFP (−0.04 vs. −0.20 %) and SRPR (0.02 vs. −0.06 %) algorithms. Compared to the results for XCO_2, the XCH_4 retrievals show larger relative scatter (0.65–0.81 %).

1 Introduction

Carbon dioxide (CO_2) and methane (CH_4) are the two most abundant anthropogenic greenhouse gases and play important roles in global warming and climate change

(IPCC, 2013). Despite their significance, there are still large gaps in our understanding of both gases concerning the spatial distribution and time dependence of their natural and anthropogenic surface sources and sinks. To get a clear comprehension of the sources and sinks of CO_2 and CH_4 requires precise continuous measurements with adequate resolution and coverage. Currently, monitoring CO_2 and CH_4 is mainly based on in-situ stations. Although these measurements provide precise results, they are limited by their spatial coverage and uneven distributions (Bousquet et al., 2006; Marquis and Tans, 2008). Besides, most of these stations are located in the boundary layer, and therefore sink estimates derived from these data are directly influenced by their sensitivity to the inversion model local vertical transport (Houweling et al., 1999; Stephens et al., 2007). The column-averaged dry-air mole fraction measurements (XCO_2 and XCH_4) are sensitive not only to the surface but also to the free troposphere, which allows a better distinction between transport and local emissions. Additionally, total column measurements are less sensitive to vertical transport and mixing, and are also representing of a larger spatial area. A large set of studies used the total column or column-averaged dry molar fraction observations to improve the precision of atmospheric inverse models (e.g. Yang et al., 2007; Keppel-Aleks et al., 2011). Recently, the satellite missions provide us with a unique view of global XCO_2 and XCH_4 distributions.

Thermal And Near infrared Sensor for carbon Observations Fourier Transform Spectrometer (TANSO-FTS) on board GOSAT was successfully launched in 2009. It is the first space-based sensor designed specifically to measure greenhouse gases from high-resolution spectra at SWIR wavelengths. The field of view of GOSAT/TANSO is about 0.0158 radian, yielding footprints that are ∼ 10.5 km in diameter at nadir (Kuze et al., 2009). So far, several algorithms have been developed to retrieve XCO_2 and XCH_4, such as University of Leicester full physics retrieval algorithm OCFP and proxy version OCPR (Boesch et al., 2011), the Netherlands Institute for Space Research/Karlsruhe Institute of Technology (SRON/KIT) full physics retrieval algorithm SRFP and proxy version SRPR (Butz et al., 2009, 2011), the NASA Atmospheric CO_2

Observations from Space or ACOS algorithm (O'Dell et al., 2012), and the National Institute for Environmental Studies (NIES) algorithm (Yoshida et al., 2011, 2013) and PPDF algorithm (Oshchepkov et al., 2008). Baker et al. (2010) and Alexe et al. (2015) pointed out that the satellite measurements of XCO_2 and XCH_4 help fill critical gaps in the in-situ network, reducing the uncertainty of the surface flux estimation. As the amplitude of the annual and seasonal variations of CO_2 and CH_4 column abundances are small compared to their mean abundances in the atmosphere, the satellite products should reach a demanding precision of 2 % or better (< 8 ppm for XCO_2 and < 34 ppb for XCH_4), in order to improve the precision of inversion models (Buchwitz et al., 2012).

It is hard to obtain reliable retrieval results over ocean in the normal nadir mode due to the low albedo in the near- and short-wave infrared spectra. Therefore, GOSAT applies the sun glint mode over the ocean at latitudes within 20° of the sub-solar latitude, in which the surface of the ocean serves as a mirror to reflect the solar radiance to the sensor directly, increasing the signal-to-noise ratio. Nowadays, the ground-based FTIR Total Carbon Column Observing Network (TCCON) has become a useful tool to validate column-averaged dry-air mole fractions of CO_2 and CH_4 (Wunch et al., 2010, 2011a). Although all the GOSAT greenhouse gases retrieval algorithms have already been validated, to some degree, via the TCCON observations (e.g. Wunch et al., 2011b; Tanaka et al., 2012; Yoshida et al., 2013; Dils et al., 2014), only the land data have been selected in these previous studies. Inoue et al. (2013) and Inoue et al. (2014) made ocean data of NIES SWIR L2 products validation by aircraft measurements. To ensure that the ocean data of GOSAT can be used to achieve a more global coverage, we compare the ocean data from different algorithms with FTIR measurements from five TCCON sites close to the ocean and near-by GOSAT land data. In Sect. 2, we introduce the GOSAT retrievals and TCCON measurements. The validation method is described in Sect. 3. The results and summary are presented in Sects. 4 and 5, respectively.

2 Data

2.1 GOSAT

For this paper, we have selected XCO_2 and XCH_4 products from the NIES v02.21, SRON/KIT v2.3.5 and ACOS v3.5 algorithms (see Table 1) with a good quality flag. To avoid the uncertainty resulting from different time coverages of each product, the selected data are limited to the April 2009 to December 2013 period.

There are two SRON/KIT algorithms, SRFP v2.3.5 and SRPR v2.3.5, which are both based on the RemoTeC algorithm. Both algorithms use the products from TANSO-CAI/GOSAT as cloud screening. SRFP is a full physics version, which adjusts parameters of surface, atmosphere and satellite instrument to fit the GOSAT spectra. SRFP also allows for the retrieval of a few effective aerosol parameters simultaneously with the CO_2 and CH_4 total column, such as particle amount, height distribution, and microphysical properties (Butz et al., 2009, 2011). While the proxy version (SRPR) of XCH_4 accounts for the scattering by taking the ratio of the XCH_4/XCO_2, so that most light-path modifications due to scattering cancel out (Schepers et al., 2012). The forward model of RemoTeC is based on the vector radiative transfer model (RTM) developed by Hasekamp and Landgraf (2005) and the Tikhonov-Phillips method is employed in the inversion scheme. Both SRFP and SRPR have applied post-processing and bias correction according to the modified version of GGG2012 (corrected for the laser sampling errors, also known as ghost issues). All data have been downloaded from the GHG-CCI project Climate Research Date Package (CRDP) database (http://www.esa-ghg-cci.org/sites/default/files/documents/public/documents/GHG-CCI_DATA.html).

NIES v02.21 also applies the cloud mask from TANSO-CAI/GOSAT products with additional cloud detection scheme only for the ocean data and retrieves aerosol parameters and surface pressure simultaneously with CO_2 and CH_4 to represent the equivalent optical path length on these cloud-screened data (Yoshida et al., 2013). The major difference between SRFP and NIES retrieval algorithms is the handling of the optical path length modification that results from the scattering. In the NIES algorithm, the state vector contains the logarithms of the mass mixing ratios of fine-mode aerosols and coarse mode aerosols, for which the a priori values are calculated by SPRINTARS V3.84 (Takemura et al., 2009). The forward model is based on the fast radiative transfer model proposed by Duan et al. (2005) and the optimal solution of the Maximum A Posteriori (MAP) method is applied as the inversion method. NIES v02.21 only contains the raw retrieval values; all data have been downloaded from https://data.gosat.nies.go.jp/.

Similar to the SRFP and NIES algorithms, ACOS v3.5 is a full-physics algorithm, but with a different cloud filtering, state vector, forward model and inversion strategy (Crisp et al., 2012; O'Dell et al., 2012). ACOS uses the information from the O_2-A band to select the clear-sky footprints (Taylor et al., 2012). The forward model is based on a fast single-scattering model (Nakajima and Tanaka, 1988), the LIDORT scalar multiple scattering model (Spurr et al., 2006), and a second-order-of scattering polarization model called 2OS (Natraj and Spurr, 2007). It fits the vertical optical depth of four scattering types together with CO_2. The modified Levenberg Marquardt method is used to minimize the cost function. As ACOS has been developed originally to retrieve the OCO satellite data products, only XCO_2 is included in the products. Wunch et al. (2011b) pointed out that the ACOS-GOSAT v2.9 XCO_2 data have a small global bias (< 0.5 ppm), and Nguyen et al. (2014) found that the ACOS v3.3 XCO_2 abundances tend to be larger than TCCON measurements by about 1–1.5 ppm. Here, the data from the latest version, ACOS v3.5, are used to compare with the "near-ocean" TCCON measurements. ACOS v3.5 products have been applied bias correction according to GGG2014.

2.2 TCCON

TCCON is a network of ground-based FTIRs targeting the provision of highly accurate and precise column-averaged dry-air mole fractions of atmospheric components including CO_2, CH_4, N_2O, HF, CO, H_2O, and HDO, for the validation of the corresponding satellite products, such as SCIAMACHY, GOSAT and OCO-2. All the TCCON stations use the GGG software to derive the gas column concentrations, as has been

described in detail by Wunch et al. (2011a). XCO_2 and XCH_4 are calculated from the ratio of the retrieved columns to the simultaneously retrieved O_2 column, so as to minimize systematic errors (Yang 2002). GGG includes its own Fourier transformation algorithm to derive the spectra from the recorded interferograms: it also corrects for the solar intensity variations during the recording of the interferogram due to the occurrence of clouds or heavy aerosol loads (Keppel-Aleks et al., 2007). Most TCCON stations have been calibrated to WMO standards by comparison to aircraft in-situ overpass measurements, and global calibration factors for each gas ($0.9898 \pm 0.001(1\sigma)$ for XCO_2 and $0.9765 \pm 0.002(1\sigma)$ for XCH_4) are applied to the TCCON data (Wunch et al., 2010; Messerschmidt et al., 2011; Tanaka et al., 2012; Geibel et al., 2012). To ensure network-wide consistency, Messerschmidt et al. (2010) and Dohe et al. (2012) discovered and minimized laser sampling errors. The latest version of GGG (GGG2014) has a ghost correction embedded in Interferogram to Spectrum (I2S) that differs in methodology to Dohe et al. (2012), but results in similar minimization of laser sampling errors (Wunch et al., 2015). Thanks to all these efforts, TCCON has already become a reliable source to validate the satellite retrievals.

As the TANSO-FTS/GOSAT sun glint data over the ocean are limited to latitudes within 20° of the sub-solar latitude, only five low-latitude and geographically close to ocean TCCON sites are selected (see Table 2, from north to south: Izaña, Ascension Island, Darwin, Reunion Island and Wollongong). The corresponding TCCON products used in this study are GGG2014 version. All data were downloaded from the TCCON Data Archive, hosted by the Carbon Dioxide Information Analysis Center (CDIAC) at tccon.ornl.gov.

3 Methodology

3.1 Spatiotemporal collocation criterion

The ideal TCCON-satellite data pair should consist of measurements at the same place during the same time. However, in order to find a sufficient number of co-located measurements to enable a robust statistical analysis, several spatiotemporal criteria were used in previous validations. Wunch et al. (2011b) used the mid tropospheric potential temperature field at 700 hPa (T700) to define the coincidence criteria, as Keppel-Aleks et al. (2011) pointed out that the potential temperature coordinate is a good proxy for large-scale CO_2 gradients in the Northern Hemisphere and mid-latitudes. Guerlet et al. (2013) utilized model CO_2 fields to determine coincidences and Nguyen et al. (2014) used a modified Euclidian distance weighted average of distance, time, and mid-Tropospheric temperature at 700 hPa. Unfortunately, in the present paper, five TCCON sites are located in the low-latitudes, where the correlation between XCO_2 gradients and potential temperature is less effective. Additionally, contrary to the relatively large amount of measurements over land, the ocean data are quite scarce. Even with a 500 or 1000 km radius collocation area around the FTIR stations, the number of TCCON-satellite data pairs turns out to be insufficient to obtain stable results.

The co-location area is finally set as ±5° latitude ±15° longitude around each TCCON site. Within this co-location box, we do not detect any significant latitude or longitude dependent bias for XCO_2 and XCH_4. Figure 1 depicts the locations of TCCON sites and co-located XCH_4 retrieval footprints from the SRPR algorithm from April 2009 to December 2013. The blue points represent the GOSAT sun glint data over ocean and the green ones correspond to the normal nadir data above land. The collocation time is set to ±2 h. That means that all the FTIR measurements occurring within ±2 h of a single satellite observation, meeting the spatial requirement, are averaged to acquire one TCCON-satellite data pair. Dils et al. (2014) demonstrated that the typical variability (1σ), of the FTIR measurements within a 4 h time window, including random errors and real atmospheric variability, is on average 2.5 ppb for XCH_4 and 0.4 ppm for XCO_2; this

meets the precision requirement of the ground-based measurements. Therefore, in the study, the statistical analyses are based on the individual data pairs or daily averaged data pairs, and all data pairs are assumed to be of equal weight.

3.2 A priori and averaging kernel corrections

Rodgers and Connor (2003) pointed out that it is not reasonable to directly compare the measurements made by different remote sounders due to their different a priori profiles and averaging kernels.

To deal with the a priori issue, TCCON a priori profile is applied as the common a priori profile to correct the satellite retrievals:

$$c_{\mathrm{cor}} = c + \sum_i h_i \left(1 - A_i^{\mathrm{sat}}\right) \left(x_{\mathrm{ap},i}^{\mathrm{TCCON}} - x_{\mathrm{ap},i}^{\mathrm{sat}}\right) \tag{1}$$

In which, c_{cor} and c are the a priori-corrected and original satellite column-averaged dry-air mole fraction; i is the vertical layer index; A_i^{sat} is the column-averaging kernel of the satellite retrieval algorithm of layer i; $x_{\mathrm{ap},i}^{\mathrm{TCCON}}$ and $x_{\mathrm{ap},i}^{\mathrm{sat}}$ are the a priori dry-air mole fraction profile of TCCON and satellite algorithm, respectively; h_i corresponds to the normalized airmass-weight function of layer i.

The prior CO_2 profile of ACOS are derived from the output of the Laboratoire de Meteorologie Dynamique (LMDz) model, with fluxes optimized to match surface observations (O'Dell et al., 2012). The prior CO_2 and CH_4 profiles of NIES are calculated for every observed day by an offline global atmospheric transport model developed by the NIES (Maksyutov et al., 2008). The a priori CO_2 profiles of SRON/KIT algorithms come from the forward run of Carbon Tracker with extrapolation based on in-situ measurements (Schepers et al., 2012), while the XCH_4 a priori is derived from the TM4 model (Meirink et al., 2006).

Figure 2 shows the impact of a priori correction for different retrieval algorithms both on ocean and land data. For each algorithm, the a priori correction factor of ocean data is similar to that of land data. For XCO_2, the correction factor (a priori corrected - original) ranges from −0.6 to 0.3 ppm. SRFP has stronger and more erratic correction factors compared to NIES and ACOS. For XCH_4, the correction factor ranges from 1.0 to 5.0 ppb with quasi-constant value at these TCCON stations.

It should be noted that we apply the spline interpolation "interpolation method" to re-grid the TCCON gas concentrations to the satellite retrieval levels or layers. It will result in errors for Izaña station, because the a priori of TCCON starts from 2.37 km, which could not cover the whole vertical range of the a priori of the satellite products. Therefore, we do the test using the same a priori of satellite retrievals below 2.37 km to do the a priori correction "fixed method". As the difference between the interpolation method and fixed method is within 0.5 ppb for XCH_4 and 0.05 ppm for XCO_2, this error can be ignored.

We have not dealt with the impact of the difference between the averaging kernels of TCCON and GOSAT data, because the true atmospheric variability is unavailable. Fortunately, the TCCON stations are located at low-latitudes, so that the solar zenith angle, during the ±2 h when GOSAT pass the TCCON sites, remains small and GOSAT and TCCON averaging kernels look very similar.

3.3 Altitude correction

Different from other stations, the Izaña FTIR is located on a steep mountain, with an altitude of 2.37 km a.s.l. If we directly compare the GOSAT data with Izaña FTIR measurements, a large bias could be generated. Therefore, in this section, we present an altitude-correction method to modify the GOSAT retrievals around the Izaña site. To that end, we calculate the ratio (α) between the column-averaged dry-air mole fractions of the target gas G above two different altitudes or pressure levels $P1$ and $P2$, based on the a priori profile shape, as

$$\alpha = c_{G,\mathrm{ak}}^{P1} / c_{G,\mathrm{ak}}^{P2}. \tag{2}$$

In Eq. (2), the column-averaged dry-air mole fraction of the target gas above pressure level $P1$, $c_{G,\mathrm{ak}}$ ($P1$), is computed as

$$c_{G,\mathrm{ak}}(P1) = \frac{VC_G(P1)}{VC_{\mathrm{air}}(P1)} = \frac{\int_{P1}^{P_{\mathrm{top}}} \frac{f_G^{\mathrm{dry}}\,\mathrm{ak}\,\mathrm{d}p}{g m_{\mathrm{air}}^{\mathrm{dry}}\left[1+f_{H_2O}^{\mathrm{dry}}\left(m_{H_2O}/m_{\mathrm{air}}^{\mathrm{dry}}\right)\right]}}{\int_{P_1}^{P_{\mathrm{top}}} \frac{\mathrm{d}p}{g m_{\mathrm{air}}^{\mathrm{dry}}\left[1+f_{H_2O}^{\mathrm{dry}}\left(m_{H_2O}/m_{\mathrm{air}}^{\mathrm{dry}}\right)\right]}}, \tag{3}$$

$$\text{with} \quad f_{H_2O}^{\mathrm{dry}} = f_{H_2O}/(1-f_{H_2O}). \tag{4}$$

In Eqs. (3) and (4) f_{H_2O} and $f_{H_2O}^{\mathrm{dry}}$ are the mole and dry-air mole fractions of H_2O, respectively, f_G^{dry} is the a priori dry-air mole fraction of the target gas G; $m_{\mathrm{air}}^{\mathrm{dry}}$ and m_{H_2O} are the molar weights of dry-air and H_2O, respectively. $P1$ and P_{top} represent the bottom and top pressure of the column, and g is the gravitational acceleration, which varies with altitude and latitude. ak stands for the averaging kernel value at pressure level p of the satellite product: it appears in order to account for the retrieval sensitivity at each pressure level in the correction factor α that we apply to the satellite data (we always apply the correction factor to the satellite product, not to the TCCON product).

To compute $f_{H_2O}^{\mathrm{dry}}$ we use the ECMWF interim reanalysis specific humidity (SH) which is given as the ratio of the mass of water vapor to the mass of moist air:

$$\mathrm{SH} = m_{H_2O} f_{H_2O} / (m_{\mathrm{air}}^{\mathrm{dry}} f_{\mathrm{air}}^{\mathrm{dry}} + m_{H_2O} f_{H_2O}), \tag{5}$$

and thus

$$f_{H_2O}^{\mathrm{dry}} = (m_{\mathrm{air}}^{\mathrm{dry}}/m_{H_2O}) \cdot \mathrm{SH}/(1-\mathrm{SH}), \tag{6}$$

Equation (3) can then be rewritten as

$$c_{G,\text{ak}}(P1) = \frac{VC_{G,\text{ak}}(P1)}{VC_{\text{air}}(P1)} = \frac{\int_{P1}^{P_\text{top}} \frac{f_G^{\text{dry}}\text{ak}\text{d}p}{gm_{\text{air}}^{\text{dry}}[1+\text{SH}/(1-\text{SH})]}}{\int_{P_1}^{P_\text{top}} \frac{\text{d}p}{gm_{\text{air}}^{\text{dry}}[1+\text{SH}/(1-\text{SH})]}}. \tag{7}$$

The correction factor α (in Eq. 2) is applied as follows:

$P1$ corresponds to the pressure level of the TCCON station and $P2$ corresponds to the pressure level of the GOSAT footprint. For example, for Izaña, the altitude of FTIR station is generally higher than that of GOSAT footprint, therefore $P1 < P2$, and the a priori profile of satellite product is used as f_G^{dry} in Eq. (7). Note that if the altitude of the GOSAT footprint is higher than the altitude of the TCCON station ($P1 > P2$), then the a priori profile of TCCON would be used as f_G^{dry}.

The corrected GOSAT retrieval product is calculated as

$$c_{\text{cor}}^{\text{alt\_cor}} = \alpha c_{\text{cor}}. \tag{8}$$

To avoid additional errors coming from the uncertainties on the gas and water vapor profiles, we applied the altitude correction only to the GOSAT products compared with the Izaña TCCON data. Figure 3 shows the time series of altitude-correction factor of XCO_2 and XCH_4 for each algorithm with its own a priori profile as f_G^{dry}. Since the concentrations decrease rapidly above the tropopause, almost all the ratios for XCH_4 are below 1. Additionally, the altitude correction factor has a seasonal variation which is caused by the seasonal variation of the tropopause height. The XCO_2 altitude-correction factors of NIES and SRFP are near 1 due to the constant vertical profile of CO_2, but the correction factor of ACOS shows a seasonal variation. This is due to the strong fluctuation in near-surface CO_2 concentrations of the a priori CO_2 profile of the ACOS algorithm.

3.4 Statistical parameters

After corrections of each TCCON-satellite data pair, several statistical parameters are derived for each of the five stations. N means the total number of co-located individual or daily averaged TCCON-satellite data pairs; R is the Pearson's correlation coefficient between the paired data; relative bias and scatter are defined as:

$$\text{relative bias} = \text{mean}(x) \times 100\,\%, \tag{9}$$

$$\text{relative scatter} = \text{SD}(x) \times 100\,\%, \tag{10}$$

$$\text{with} \quad x = (X_{\text{TCCON}} - X_{\text{SAT}})/X_{\text{TCCON}}. \tag{11}$$

In which XTCCON(SAT) stands for the TCCON or satellite data product, respectively. We assume that relative bias follows a Gaussian distribution, and then, the 95 % confidence interval of bias is computed as:

$$(\overline{x} - s/\sqrt{n} \cdot t_{0.025}(n-1), \overline{x} + s/\sqrt{n} \cdot t_{0.025}(n-1)), \tag{12}$$

$$s = \sqrt{\frac{1}{n-1}\sum_{i=1}^{n}(x_i - \overline{x})^2}. \tag{13}$$

Here, t represents the t distribution, s is the sample standard deviation (relative scatter), n is the sample size (the number of individual TCCON-satellite data pairs).

4 Results

After a priori and altitude correction, the time series of GOSAT retrievals and TCCON measurements are shown in Figs. 4 and 6 and the statistics are listed in Tables 3 and 4, for XCO_2 and XCH_4, respectively. In the Figures, red points represent the FTIR measurements, blue and green ones correspond to the GOSAT sun glint data over ocean and the normal nadir data above land, respectively.

4.1 XCO_2

For XCO_2, the products of three full-physics algorithms (NIES, SRFP and ACOS) have been compared with the TCCON FTIR measurements. In general, both ocean and land data of all algorithms show good agreement with FTIR measurements, capturing the seasonal and annual variations of XCO_2. There are several data gaps at each site mainly due to missing TCCON measurements.

Table 3 summarizes the ocean and land statistical results for 5 TCCON stations based on all individual TCCON-satellite pairs. Between the brackets are the results without altitude correction. At each site, the relative biases of all algorithms are within 0.6 % and scatters are within 0.7 %. Averaged over all TCCON sites (taking all the individual data), the relative biases of ocean data and land data with 95 % confidence bands are 0.33 ± 0.018 and 0.13 ± 0.013 % for NIES, −0.03 ± 0.026 and −0.04 ± 0.012 % for SRFP, −0.06 ± 0.011 and 0.03 ± 0.008 % for ACOS. The correlation between GOSAT ocean and FTIR data is better than that between GOSAT land and FTIR data, and the scatter for the GOSAT ocean data is smaller than that for the land data. Although the altitude difference is not so crucial for XCO_2, the biases at Izaña become smaller after altitude correction, especially for ocean data. ACOS provides the largest data density both for land and ocean retrievals and NIES has more ocean data but less land data than SRFP.

The sub-solar latitude changes throughout the year, consequently, the glint ocean data around each TCCON station only exist in several specific months. To better compare the ocean data and land data, we choose the GOSAT soundings when both data co-exist within ±1 day. Figure 5 shows the scatter plots of daily median of XCO_2 from FTIR measurements and different GOSAT algorithms retrievals over five TCCON stations. The error bar represents the standard deviation of all the measurements during ±1 day. Due to the unavailability of land data, only ocean data are shown at Ascension. It is clear that the ocean XCO_2 of NIES is smaller than the land XCO_2 or FTIR measurements at Izaña, Ascension, Reunion and Wollongong. For SRPF and ACOS,

the accuracy of the ocean data is close to that of the land data and the scatter of the ocean data is even less than that of the land data. However, it is found that the land data of SRFP at Izaña have a larger bias than those of NIES and ACOS. As the land data around Izaña are located above the Saharan desert, the reason probably is that the scattering model applied by SRFP could not account correctly for the dust aerosol in the atmosphere, or it could be due to the fact that the gain *M* bias correction of SRFP is mostly based on comparison with TCCON stations in Australia.

4.2 XCH_4

Figure 6 shows the time series of GOSAT XCH_4 retrievals from NIES, SRFP and SRPR together with TCCON FTIR measurements. At first glance, similar to the results of XCO_2, both ocean and land data of all algorithms show good agreement with FTIR measurements. Note that it has been found that there is a systematic underestimation of SRPR XCH_4 in December 2013 (∼ 10 ppb) due to an error in the XCO_2 priori for that month (not shown). Therefore, SRPR products for that month have been eliminated. Large variations at the Wollongong site (see Fig. 6) indicate that there are local methane emissions nearby, which was already demonstrated by Fraser et al. (2011). They pointed out that emissions from coal mining are the largest source of methane above background levels at Wollongong, accounting for 60 % of the surface concentration. As the GOSAT retrievals from all algorithms also see these variations, the emissions probably cover a large area.

Table 4 lists the statistical results for XCH_4. All the biases for ocean and land data at all sites are within 0.8 %, and the scatters are within 1.0 %; this means that they meet the single precision threshold quality criteria for inverse modeling (34 ppb XCH_4). Although SRFP and SRPR are both derived from the RemoTeC algorithm, the proxy version (SRPR) has a larger data density than the full physics version (SRFP) because with the latter, a post-filter is applied that sets a threshold on the scattering parameters (Butz et al., 2010). Averaged over all TCCON sites, the relative bias with 95 % confidence intervals of ocean data is less than that of the land data for NIES (−0.02 ± 0.032

vs. 0.35 ± 0.019 %), SRFP (−0.04 ± 0.051 vs. −0.20 ± 0.018 %) and SRPR (0.02 ± 0.028 vs. −0.06 ± 0.012 %). It is found that the XCH_4 products of SRFP have a smaller data density than the XCO_2 products for ocean data, which means that some extra filter was applied to the XCH_4 retrievals.

Note that it is indispensable to do altitude correction when comparing the GOSAT XCH_4 retrievals with the FTIR measurements for Izaña. The altitude-corrected biases between the GOSAT and FTIR are smaller than the ones obtained without altitude correction, and show similar scatter and higher correlation coefficient. The bias decrease for ocean data is larger than that for land data (1.17 and 0.95 % for NIES, 1.21 and 1.08 % for SRFP, 1.20 and 0.94 % for SRPR), because the GOSAT footprints over ocean have a lower altitude; this could also be recognized in the time series of altitude-correction factors (see Fig. 3).

Figure 7 shows the scatter plots of XCH_4 daily median of FTIR measurements and different GOSAT retrievals over TCCON sites. As in Fig. 5, it is found that the land data of SRFP at Izaña have large bias and scatter. As mentioned at Sect. 4.1, this error probably results from the dust aerosol in the air. Apart from that, the XCH_4 abundances of ocean data at Darwin are larger than the FTIR measurements, and the biases range from −0.30 to -0.59 % for these three algorithms. This systematic bias may originate in the fact that almost all the ocean footprints near Darwin site are limited to a small area (near 125° E, see Fig. 1), and are a little bit further away from the FTIR location compared with the distances at the other four sites. For the other sites, the accuracy of ocean data of the three algorithms is close to that of the land data.

4.3 Stability

Figure 8 shows the annual mean biases and corresponding standard deviations of the ocean data from the different algorithms and molecules at each TCCON station, based on individual co-located ocean data pairs. Almost all annual mean biases are within 1 % during the measurement period 2009–2013 and the differences between adjacent years at are within 0.4 % for XCO_2 and 0.7 % for XCH_4 at each station. The maximum

differences between each station in the same year are about 0.3 % for XCO_2 and 1.1 % for XCH_4. The XCO_2 ocean data from ACOS seem more stable than the NIES and SRFP data; their biases are close to 0 and the standard deviations are smaller. The XCO_2 ocean data from NIES have a systematic bias, and their standard deviations are similar to those of SPFP. The stability of XCH_4 ocean data from SRFP tends to be slightly better than that from NIES and SRPR, but one should keep in mind that the XCH_4 data from SRFP algorithm have the lowest data density.

5 Summary

The XCO_2 and XCH_4 GOSAT sun glint mode retrievals from NIES v02.21, SRFP v2.3.5, SRPR v2.3.5 and ACOS v3.5 algorithms were validated with the FTIR measurements from five TCCON stations and nearby GOSAT land data. As the GOSAT land data have already been validated with TCCON measurements in previous studies, we mainly focused on the differences between ocean data and near-by land data. Due to the low data density of sun glint mode retrievals, all the GOSAT footprints located within ±5° latitude and ±15° longitude around each TCCON site were selected. The a priori profile of TCCON is used as the common profile to eliminate the differences between GOSAT and FTIR data due to the use of different a priori profiles in their retrievals. An altitude-correction method is applied to eliminate the bias due to altitude differences between the FTIR station location and the GOSAT footprints, but only in the comparisons made at Izaña; it is particularly important when comparing the XCH_4 data.

For XCO_2, NIES, SRFP and ACOS algorithms are all full-physics methods but with different cloud filters, forward models and inversion schemes. ACOS provides the largest data density both for land and ocean products and NIES has more ocean data but less land data than SRFP. Averaged over all TCCON sites, the relative biases of ocean data and land data with 95 % confidence intervals are 0.33 ± 0.018 and 0.13 ± 0.013 % for NIES, −0.03 ± 0.026 and −0.04 ± 0.012 % for SRFP, −0.06 ± 0.011

and 0.03 ± 0.008 % for ACOS, respectively. Apart from the XCO_2 ocean data from NIES indicating a slight systematic bias, other retrievals show good agreement with TCCON measurements, among which the ACOS products have the most robust stability.

For all algorithms, the XCH_4 retrievals have a worse stability and smaller precision than the XCO_2 retrievals. Although the SRPR and SRFP are both derived from the RemoTeC algorithm, SRPR provides more data, and its ocean data show a larger scatter. The lower density of SRFP ocean data probably results from the application of a severe cloud and aerosol post-filtering. Averaged over all 5 TCCON sites, the relative bias with 95 % confidence intervals of ocean data is less than that of the land data for NIES (−0.02 ± 0.032 vs.0.35 ± 0.019 %), SRFP (−0.04 ± 0.051 vs. −0.20 ± 0.018 %) and SRPR (0.02 ± 0.028 vs. −0.06 ± 0.012 %).

Acknowledgement. This work is supported by the National Natural Science Foundation of China (41575034) and the National Basic Research Program of China (2013CB955801) and the Belgian contribution by the ESA Climate Change Initiative-Greenhouse Gases project. The TCCON measurements at Ile de La Reunion are supported by the EU FP7 project ICOS_Inwire, as well as the Belgian support to ICOS and to the AGACCII project of the Science for Sustainable Development programme. The TCCON station on Ascension Island has been funded by the Max Planck Institute for Biogeochemistry. The operation of the Izaña FTIR instrument has been very importantly supported by O. E. García and E. Sepúlveda, which are contracted by the Meteorological State Agency of Spain (AEMET). Measurements at Darwin and Wollongong are supported by Australian Research Council grants DP0879468, DP110103118 & DP140101552. Darwin TCCON is also supported by the Australian Bureau of Meteorology and NASA's Orbiting Carbon Observatory Project. TCCON data were obtained from the TCCON Data Archive, hosted by the Carbon Dioxide Information Analysis Center (CDIAC)-tccon.ornl.gov. The ACOS/GOSAT retrievals were developed and carried out at the NASA Jet Propulsion Laboratory and Colorado State University, with funding from the NASA ACOS project. The SRON/GOSAT has been supported by the ESA Climate Change Initiative-Greenhouse Gases project. The authors thank D. Wunch for useful comments to the manuscript.

References

Alexe, M., Bergamaschi, P., Segers, A., Detmers, R., Butz, A., Hasekamp, O., Guerlet, S., Parker, R., Boesch, H., Frankenberg, C., Scheepmaker, R. A., Dlugokencky, E., Sweeney, C., Wofsy, S. C., and Kort, E. A.: Inverse modelling of CH_4 emissions for 2010–2011 using different satellite retrieval products from GOSAT and SCIAMACHY, Atmos. Chem. Phys., 15, 113–133, doi:10.5194/acp-15-113-2015, 2015.

Baker, D. F., Bösch, H., Doney, S. C., O'Brien, D., and Schimel, D. S.: Carbon source/sink information provided by column CO_2 measurements from the Orbiting Carbon Observatory, Atmos. Chem. Phys., 10, 4145–4165, doi:10.5194/acp-10-4145-2010, 2010.

Blumenstock, T., Hase, F., Schneider, M., García, O. E., and Sepúlveda, E.: TCCON data from Izaña, Tenerife, Spain, Release GGG2014R0, TCCON data archive, hosted by the Carbon Dioxide Information Analysis Center, Oak Ridge National Laboratory, Oak Ridge, Tennessee, USA, doi:10.14291/tccon.ggg2014.izana01.R0/1149295, doi:10.14291/tccon.ggg2014.izana01.R0/1149295, 2014.

Boesch, H., Baker, D., Connor, B., Crisp, D., and Miller, C.: Global characterization of CO_2 column retrievals from shortwave-infrared satellite observations of the orbiting carbon observatory-2 mission, Remote Sens., 3, 270–304, doi:10.3390/rs3020270, 2011.

Bousquet, P., Ciais, P., Miller, J. B., Dlugokencky, E. J., Hauglustaine, D. A., Prigent, C., Van der Werf, G. R., Peylin, P., Brunke, E.-G., Carouge, C., Langenfelds, R. L., Lathiere, J., Papa, F., Ramonet, M., Schmidt, M., Steele, L. P., Tyler, S. C., and White, J.: Contribution of anthropogenic and natural sources to atmospheric methane variability, Nature, 443, 439–443, doi:10.1038/nature05132, 2006.

Buchwitz, M., Chevallier, F., and Bergamaschi, P.: User Requirements Document (URD) for the GHG-CCI project of ESA's Climate Change Initiative, Technical Report, 45 pp., version 1(URDv1), 3 February 2011, available at: http://www.esa-ghg-cci.org/?q=webfm_send/21 (last access: 5 June 2014), 2012.

Butz, A., Hasekamp, O. P., Frankenberg, C., and Aben, I.: Retrievals of atmospheric CO_2 from simulated space-borne measurements of backscattered near-infrared sunlight: accounting for aerosol effects, Appl. Optics, 48, 3322–3336, doi:10.1364/AO.48.003322, 2009.

Butz, A., Hasekamp, O. P., Frankenberg, C., Vidot, J., and Aben, I.: CH_4 retrievals from space-based solar backscatter measurements: performance evaluation against simulated aerosol and cirrus loaded scenes, J. Geophys. Res., 115, D24302, doi:10.1029/2010jd014514, 2010.

Butz, A., Guerlet, S., Hasekamp, O., Schepers, D., Galli, A., Aben, I., Frankenberg, C., Hartmann, J.-M., Tran, H., Kuze, A., Keppel-Aleks, G., Toon, G., Wunch, D., Wennberg, P., Deutscher, N., Griffith, D., Macatangay, R., Messerschmidt, J., Notholt, J., and Warneke, T.: Toward accurate CO_2 and CH_4 observations from GOSA T, Geophys. Res. Lett., 38, L14812, doi:10.1029/2011gl047888, 2011.

Crisp, D., Breon, F. M., Brown, L. R., Burrows, J. P., Ciais, P., Connor, B. J., Doney, S. C., Fung, I. Y., Jacob, D. J., Miller, C. E., O'Brien, D., Pawson, S., Randerson, J. T., Rayner, P., Salawitch, R. J., Sander, S. P., Sen, B., Stephens, G. L., Tans, P. P., Toon, G. C., Wennberg, P. O., Wofsy, S. C., Yung, Y. L., Kuang, Z., Chudasama, B., Sprague, G., Weiss, B., Pollock, R., Kenyon, D., and Schroll, S.: The orbiting carbon observatory (OCO) mission. Adv. Space Res., 34, 700–709, doi:10.1016/j.asr.2003.08.062, 2004.

Crisp, D., Fisher, B. M., O'Dell, C., Frankenberg, C., Basilio, R., Bösch, H., Brown, L. R., Castano, R., Connor, B., Deutscher, N. M., Eldering, A., Griffith, D., Gunson, M., Kuze, A., Mandrake, L., McDuffie, J., Messerschmidt, J., Miller, C. E., Morino, I., Natraj, V., Notholt, J., O'Brien, D. M., Oyafuso, F., Polonsky, I., Robinson, J., Salawitch, R., Sherlock, V., Smyth, M., Suto, H., Taylor, T. E., Thompson, D. R., Wennberg, P. O., Wunch, D., and Yung, Y. L.: The ACOS CO_2 retrieval algorithm – Part II: Global XCO_2 data characterization, Atmos. Meas. Tech., 5, 687–707, doi:10.5194/amt-5-687-2012, 2012.

De Mazière, M., Sha, M. K., Desmet, F., Hermans, C., Scolas, F., Kumps, N., Metzger, J.-M., Duflot, V., and Cammas, J.-P.: TCCON data from Réunion Island, France, Release GGG2014R0, TCCON data archive, hosted by the Carbon Dioxide Information Analysis Center, Oak Ridge National Laboratory, Oak Ridge, Tennessee, USA, doi:10.14291/tccon.ggg2014.reunion01.R0/1149288, doi:10.14291/tccon.ggg2014.reunion01.R0/1149288, 2014.

Dils, B., Buchwitz, M., Reuter, M., Schneising, O., Boesch, H., Parker, R., Guerlet, S., Aben, I., Blumenstock, T., Burrows, J. P., Butz, A., Deutscher, N. M., Frankenberg, C., Hase, F., Hasekamp, O. P., Heymann, J., De Mazière, M., Notholt, J., Sussmann, R., Warneke, T., Griffith, D., Sherlock, V., and Wunch, D.: The Greenhouse Gas Climate Change Initiative (GHG-CCI): comparative validation of GHG-CCI SCIAMACHY/ENVISAT and TANSO-FTS/GOSAT CO_2 and CH_4 retrieval algorithm products with measurements from the TCCON, Atmos. Meas. Tech., 7, 1723–1744, doi:10.5194/amt-7-1723-2014, 2014.

Dohe, S., Sherlock, V., Hase, F., Gisi, M., Robinson, J., Sepúlveda, E., Schneider, M., and Blumenstock, T.: A method to correct sampling ghosts in historic near-infrared Fourier transform spectrometer (FTS) measurements, Atmos. Meas. Tech., 6, 1981–1992, doi:10.5194/amt-6-1981-2013, 2013.

Duan, M., Min, Q., and Li, J.: A fast radiative transfer model for simulating high-resolution absorption bands, J. Geophys. Res., 110, D15201, doi:10.1029/2004JD005590, 2005.

Feist, D. G., Arnold, S. G., John, N., and Geibel, M. C.: TCCON data from Ascension Island, Saint Helena, Ascension and Tristan da Cunha, Release GGG2014R0, TCCON data archive, hosted by the Carbon Dioxide Information Analysis Center, Oak Ridge National Laboratory, Oak Ridge, Tennessee, USA, doi:10.14291/tccon.ggg2014.ascension01.R0/1149285, doi:10.14291/tccon.ggg2014.ascension01.R0/1149285, 2014.

Fraser, A., Chan Miller, C., Palmer, P. I., Deutscher, N. M., Jones, N. B., and Griffith D. W. T.: The Australian methane budget: interpreting surface and train-borne measurements using a chemistry transport model, J. Geophys. Res., 116, D20306, doi:10.1029/2011JD015964, 2011.

Geibel, M. C., Messerschmidt, J., Gerbig, C., Blumenstock, T., Chen, H., Hase, F., Kolle, O., Lavrič, J. V., Notholt, J., Palm, M., Rettinger, M., Schmidt, M., Sussmann, R., Warneke, T., and Feist, D. G.: Calibration of column-averaged CH_4 over European TCCON FTS sites with airborne in-situ measurements, Atmos. Chem. Phys., 12, 8763–8775, doi:10.5194/acp-12-8763-2012, 2012.

Griffith, D. W. T., Deutscher, N., Velazco, V. A., Wennberg, P. O., Yavin, Y., Keppel Aleks, G., Washenfelder, R., Toon, G. C., Blavier, J.-F., Murphy, C., Jones, N., Kettlewell, G., Connor, B., Macatangay, R., Roehl, C., Ryczek, M., Glowacki, J., Culgan, T., and Bryant, G.: TCCON data from Darwin, Australia, Release GGG2014R0, TCCON data archive, hosted by the Carbon Dioxide Information Analysis Center, Oak Ridge National Laboratory, Oak Ridge, Tennessee, USA, doi:10.14291/tccon.ggg2014.darwin01.R0/1149290, doi:10.14291/tccon.ggg2014.darwin01.R0/1149290, 2014a.

Griffith, D. W. T., Velazco, V. A., Deutscher, N., Murphy, C., Jones, N., Wilson, S., Macatangay, R., Kettlewell, G., Buchholz, R. R., and Riggenbach, M.: TCCON data from Wollongong, Australia, Release GGG2014R0, TCCON data archive, hosted by the Carbon Dioxide Information Analysis Center, Oak Ridge National Laboratory, Oak Ridge, Tennessee, USA, doi:10.14291/tccon.ggg2014.wollongong01.R0/1149291, doi:10.14291/tccon.ggg2014.wollongong01.R0/1149291, 2014b.

Discussion Paper | Discussion Paper | Discussion Paper | Discussion Paper |

Guerlet, S., Butz, A., Schepers, D., Basu, S., Hasekamp, O. P., Kuze, A., Yokota, T., Blavier, J.-F., Deutscher, N. M., Griffith, D. W., Hase, F., Kyro, E., Morino, I., Sherlock, V., Sussmann, R., Galli, A., and Aben, I.: Impact of aerosol and thin cirrus on retrieving and validating XCO_2 from GOSAT shortwave infrared measurements, J. Geophys. Res.-Atmos., 118, 4887–4905, 2013.

Hasekamp, O. P. and Landgraf, J.: Linearization of vector radiative transfer with respect to aerosol properties and its use in satellite remote sensing, J. Geophys. Res., 110, D04203, doi:10.1029/2004JD005260, 2005.

Houweling, S., Kaminski, T., Dentener, F., Lelieveld, J., and Heimann, M.: Inverse modeling of methane sources and sinks using the adjoint of a global transport model, J. Geophys. Res., 104, 26137–26160, 1999.

Inoue, M., Morino, I., Uchino, O., Miyamoto, Y., Yoshida, Y., Yokota, T., Machida, T., Sawa, Y., Matsueda, H., Sweeney, C., Tans, P. P., Andrews, A. E., Biraud, S. C., Tanaka, T., Kawakami, S., and Patra, P. K.: Validation of XCO_2 derived from SWIR spectra of GOSAT TANSO-FTS with aircraft measurement data, Atmos. Chem. Phys., 13, 9771–9788, doi:10.5194/acp-13-9771-2013, 2013.

Inoue, M., Morino, I., Uchino, O., Miyamoto, Y., Saeki, T., Yoshida, Y., Yokota, T., Sweeney, C., Tans, P. P., Biraud, S. C., Machida, T., Pittman, J. V., Kort, E. A., Tanaka, T., Kawakami, S., Sawa, Y., Tsuboi, K., and Matsueda, H.: Validation of XCH_4 derived from SWIR spectra of GOSAT TANSO-FTS with aircraft measurement data, Atmos. Meas. Tech., 7, 2987–3005, doi:10.5194/amt-7-2987-2014, 2014.

IPCC, 2013: Climate Change 2013: The Physical Science Basis. Contribution of Working Group I to the Fifth Assessment Report of the Intergovernmental Panel on Climate Change, edited by: Stocker, T. F., Qin, D., Plattner, G.-K., Tignor, M., Allen, S. K., Boschung, J., Nauels, A., Xia, Y., Bex, V., and Midgley P. M., Cambridge University Press, Cambridge, UK and NY, USA, doi:10.1017/CBO9781107415324, 2013.

Keppel-Aleks, G., Toon, G. C., Wennberg, P. O., and Deutscher, N.: Reducing the impact of source brightness fluctuations on spectra obtained by FTS, Appl. Optics, 46, 4774–4779, doi:10.1364/AO.46.004774, 2007.

Keppel-Aleks, G., Wennberg, P. O., and Schneider, T.: Sources of variations in total column carbon dioxide, Atmos. Chem. Phys., 11, 3581–3593, doi:10.5194/acp-11-3581-2011, 2011.

Kuze, A., Suto, H., Nakajima, M., and Hamazaki, T.: Thermal and near infrared sensor for carbon observation Fourier-transform spectrometer on the Greenhouse Gases

Observing Satellite for greenhouse gases monitoring, Appl. Optics, 48, 6716–6733, doi:10.1364/AO.48.006716, 2009.

Maksyutov, S., Patra, P. K., Onishi, R., Saeki, T., and Nakazawa, T.: NIES/FRCGC global atmospheric tracer transport model: Description, validation, and surface sources and sinks inversion, Journal of the Earth Simulator, 9, 3–18, 2008.

Marquis, M. and Tans, P.: Carbon Crucible, Science, 320, 460–461, doi:10.1126/science.1156451, 2008.

Messerschmidt, J., Macatangay, R., Notholt, J., Petri, C., Warneke, T., and Weinzierl, C.: Side by side measurements of CO_2 by ground-based Fourier transform spectrometry (FTS), Tellus B, 62, 749–758, doi:10.1111/j.1600-0889.2010.00491.x, 2010.

Messerschmidt, J., Geibel, M. C., Blumenstock, T., Chen, H., Deutscher, N. M., Engel, A., Feist, D. G., Gerbig, C., Gisi, M., Hase, F., Katrynski, K., Kolle, O., Lavrič, J. V., Notholt, J., Palm, M., Ramonet, M., Rettinger, M., Schmidt, M., Sussmann, R., Toon, G. C., Truong, F., Warneke, T., Wennberg, P. O., Wunch, D., and Xueref-Remy, I.: Calibration of TCCON column-averaged CO_2: the first aircraft campaign over European TCCON sites, Atmos. Chem. Phys., 11, 10765–10777, doi:10.5194/acp-11-10765-2011, 2011.

Nakajima, T. and Tanaka, M.: Algorithms for radiative intensity calculations in moderately thick atmospheres using a truncation approximation, J. Quant. Spectrosc. Ra., 40, 51–69, doi:10.1016/0022-4073(88)90031-3, 1988.

Natraj, V. and Spurr, R. J. D.: A fast linearized pseudo-spherical two orders of scattering model to account for polarization in vertically inhomogeneous scattering absorbing media, J. Quant. Spectrosc. Ra., 107, 263–293, doi:10.1016/j.jqsrt.2007.02.011, 2007.

Nguyen, H., Osterman, G., Wunch, D., O'Dell, C., Mandrake, L., Wennberg, P., Fisher, B., and Castano, R.: A method for colocating satellite XCO_2 data to ground-based data and its application to ACOS-GOSAT and TCCON, Atmos. Meas. Tech., 7, 2631–2644, doi:10.5194/amt-7-2631-2014, 2014.

O'Dell, C. W., Connor, B., Bösch, H., O'Brien, D., Frankenberg, C., Castano, R., Christi, M., Eldering, D., Fisher, B., Gunson, M., McDuffie, J., Miller, C. E., Natraj, V., Oyafuso, F., Polonsky, I., Smyth, M., Taylor, T., Toon, G. C., Wennberg, P. O., and Wunch, D.: The ACOS CO_2 retrieval algorithm – Part 1: Description and validation against synthetic observations, Atmos. Meas. Tech., 5, 99–121, doi:10.5194/amt-5-99-2012, 2012.

Oshchepkov, S., Bril, A., and Yokota, T.: PPDF-based method to account for atmospheric light scattering in observations of carbon dioxide from space, J. Geophys. Res., 113, D23210, doi:10.1029/2008JD010061, 2008.

Rodgers, C. D. and Connor, B. J.: Intercomparison of remote sounding instruments, J. Geophys. Res., 108, D3, doi:10.1029/2002jd002299, 2003.

Schepers, D., Guerlet, S., Butz, A., Landgraf, J., Frankenberg, C., Hasekamp, O., Blavier, J. F., Deutscher, N., M. Griffith, D. W. T., Hase, F., Kyro, E., Morino, I., Sherlock, V., Sussmann, R., and Aben, I.: Methane retrievals from Greenhouse Gases Observing Satellite (GOSAT) shortwave infrared measurements: Performance comparison of proxy and physics retrieval algorithms, J. Geophys. Res., 117, D10, doi:10.1029/2012jd017549, 2012.

Spurr, R. J. D., Kurosu, T. P., and Chance, K. V.: A linearized discrete ordinate radiative transfer model for atmospheric remote-sensing retrieval, J. Quant. Spectrosc. Ra., 68, 689–735, doi:10.1016/S0022-4073(00)00055-8, 2001.

Stephens, B. B., Gurney, K. R., Tans, P. P., Sweeney, C., Peters, W., Bruhwiler, L., Ciais, P., Ramonet, M., Bousquet, P., Nakazawa, T., Aoki, S., Machida, T., Inoue, G., Vinnichenko, N., Lloyd, J., Jordan, A., Heimann, M., Shibistova, O., Langenfelds, R. L., Steele, L. P., Francey, R. J., and Denning, A. S.: Weak northern and strong tropical land carbon Uptake from vertical profiles of atmospheric CO_2, Science, 316, 1732–1735, doi:10.1126/science.1137004, 2007.

Takemura, T., Egashira, M., Matsuzawa, K., Ichijo, H., O'ishi, R., and Abe-Ouchi, A.: A simulation of the global distribution and radiative forcing of soil dust aerosols at the Last Glacial Maximum, Atmos. Chem. Phys., 9, 3061–3073, doi:10.5194/acp-9-3061-2009, 2009.

Tanaka, T., Miyamoto, Y., Morino, I., Machida, T., Nagahama, T., Sawa, Y., Matsueda, H., Wunch, D., Kawakami, S., and Uchino, O.: Aircraft measurements of carbon dioxide and methane for the calibration of ground-based high-resolution Fourier Transform Spectrometers and a comparison to GOSAT data measured over Tsukuba and Moshiri, Atmos. Meas. Tech., 5, 2003–2012, doi:10.5194/amt-5-2003-2012, 2012.

Taylor, T. E., O'Dell, C. W., O'Brien, D. M., Kikuchi, N., Yokota, T., Nakajima, T. Y., Ishida, H., Crisp, D., and Nakajima, T.: Comparison of Cloud-Screening Methods Applied to GOSAT Near-Infrared Spectra, IEEE T. Geosci. Remote, 50, 295–309, doi:10.1109/TGRS.2011.2160270, 2012.

Wunch, D., Toon, G. C., Wennberg, P. O., Wofsy, S. C., Stephens, B. B., Fischer, M. L., Uchino, O., Abshire, J. B., Bernath, P., Biraud, S. C., Blavier, J.-F. L., Boone, C., Bow-

man, K. P., Browell, E. V., Campos, T., Connor, B. J., Daube, B. C., Deutscher, N. M., Diao, M., Elkins, J. W., Gerbig, C., Gottlieb, E., Griffith, D. W. T., Hurst, D. F., Jiménez, R., Keppel-Aleks, G., Kort, E. A., Macatangay, R., Machida, T., Matsueda, H., Moore, F., Morino, I., Park, S., Robinson, J., Roehl, C. M., Sawa, Y., Sherlock, V., Sweeney, C., Tanaka, T., and Zondlo, M. A.: Calibration of the Total Carbon Column Observing Network using aircraft profile data, Atmos. Meas. Tech., 3, 1351–1362, doi:10.5194/amt-3-1351-2010, 2010.

Wunch, D., Toon, G. C., Blavier, J. F., Washenfelder, R. A., Notholt, J., Connor, B. J., Griffith, D. W., Sherlock, V., and Wennberg, P. O.: The total carbon column observing network, Philos. T. Roy. Soc. A., 369, 2087–2112, doi:10.1098/rsta.2010.0240, 2011a.

Wunch, D., Wennberg, P. O., Toon, G. C., Connor, B. J., Fisher, B., Osterman, G. B., Frankenberg, C., Mandrake, L., O'Dell, C., Ahonen, P., Biraud, S. C., Castano, R., Cressie, N., Crisp, D., Deutscher, N. M., Eldering, A., Fisher, M. L., Griffith, D. W. T., Gunson, M., Heikkinen, P., Keppel-Aleks, G., Kyrö, E., Lindenmaier, R., Macatangay, R., Mendonca, J., Messerschmidt, J., Miller, C. E., Morino, I., Notholt, J., Oyafuso, F. A., Rettinger, M., Robinson, J., Roehl, C. M., Salawitch, R. J., Sherlock, V., Strong, K., Sussmann, R., Tanaka, T., Thompson, D. R., Uchino, O., Warneke, T., and Wofsy, S. C.: A method for evaluating bias in global measurements of CO_2 total columns from space, Atmos. Chem. Phys., 11, 12317–12337, doi:10.5194/acp-11-12317-2011, 2011b.

Wunch, D., Toon, G. C., Sherlock, V., Deutscher, N. M., Liu, X., Feist, D. G., and Wennberg P. O.: The Total Carbon Column Observing Network GGG2014 Data Version. Carbon Dioxide Information Analysis Center, Oak Ridge National Laboratory, Oak Ridge, Tennessee, USA, doi:10.14291/tccon.ggg2014.documentation.R0/1221662, 2015.

Yang, Z.: Atmospheric CO_2 retrieved from ground-based near IR solar spectra, Geophys. Res. Lett., 29, 53-1–53-4, doi:10.1029/2001gl014537, 2002.

Yang, Z., Washenfelder, R. A., Keppel-Aleks, G., Krakauer, N. Y., Randerson, J. T., Tans, P. P., Sweeney, C., and Wennberg, P. O.: New constraints on Northern Hemisphere growing season net flux, Geophys. Res. Lett., 34, L12807, doi:10.1029/2007GL029742, 2007.

Yokota, T., Yoshida, Y., Eguchi, N., Ota, Y., Tanaka, T., Watanabe, H., and Maksyutov, S.: Global Concentrations of CO_2 and CH_4, retrieved from GOSAT: first preliminary results, Sci. Online Lett. Atmos., 5, 160–163, doi:10.2151/sola.2009-041, 2009.

Yoshida, Y., Ota, Y., Eguchi, N., Kikuchi, N., Nobuta, K., Tran, H., Morino, I., and Yokota, T.: Retrieval algorithm for CO_2 and CH_4 column abundances from short-wavelength infrared

spectral observations by the Greenhouse gases observing satellite, Atmos. Meas. Tech., 4, 717–734, doi:10.5194/amt-4-717-2011, 2011.
Yoshida, Y., Kikuchi, N., Morino, I., Uchino, O., Oshchepkov, S., Bril, A., Saeki, T., Schutgens, N., Toon, G. C., Wunch, D., Roehl, C. M., Wennberg, P. O., Griffith, D. W. T., Deutscher, N. M., Warneke, T., Notholt, J., Robinson, J., Sherlock, V., Connor, B., Rettinger, M., Sussmann, R., Ahonen, P., Heikkinen, P., Kyrö, E., Mendonca, J., Strong, K., Hase, F., Dohe, S., and Yokota, T.: Improvement of the retrieval algorithm for GOSAT SWIR XCO_2 and XCH_4 and their validation using TCCON data, Atmos. Meas. Tech., 6, 1533–1547, doi:10.5194/amt-6-1533-2013, 2013.

Table 1. TANSO-FTS/GOSAT retrieval algorithms.

Molecular	Algorithm	Institute	Time period	References
XCO_2	NIES v02.21	NIES	04/2009–05/2014	Yoshida et al. (2011, 2013)
	SRFP v2.3.5	SRON/KIT	04/2009–12/2013	Butz et al. (2011)
	ACOS v3.5	NASA	04/2009–06/2014	O'Dell et al. (2012)
XCH_4	NIES v02.21	NIES	04/2009–05/2014	Yoshida et al. (2011, 2013)
	SRFP v2.3.5	SRON/KIT	04/2009–12/2013	Butz et al. (2011)
	SRPR v2.3.5	SRON/KIT	04/2009–12/2013	Schepers et al. (2012)

Discussion Paper | Discussion Paper | Discussion Paper | Discussion Paper |

Table 2. The locations and start times of TCCON sites.

Site	Latitude	Longitude	Alt (km a.s.l)	Start time	References
Izaña	28.3° N	16.5° W	2.37	May 2007	Blumenstock et al. (2014)
Ascension Island	7.9° S	14.3° W	0.01	May 2012	Feist et al. (2014)
Darwin	12.4° S	130.9° E	0.03	Aug 2005	Griffith et al. (2014a)
Reunion Island	20.9° S	55.5° E	0.09	Sep 2011	De Mazière et al. (2014)
Wollongong	34.4° S	150.8° E	0.03	May 2008	Griffith et al. (2014b)

Table 3. XCO_2 results of NIES, SRFP and ACOS algorithms at 5 TCCON stations based on all individual TCCON-satellite data pairs. The 95 % confidence interval of relative bias, relative scatter, R and N are defined in Sect. 3.4. Between brackets are the results without altitude correction.

Site	Target	NIES_XCO_2				SRFP_XCO_2				ACOS_XCO_2			
		95 % Bias	Scatter	R	N	95 % Bias	Scatter	R	N	95 % Bias	Scatter	R	N
Iza	Ocean	0.24 ± 0.036 (0.27 ± 0.038)	0.37 (0.39)	0.88 (0.88)	397	−0.05 ± 0.052 (−0.07 ± 0.056)	0.38 (0.41)	0.92 (0.91)	205	−0.09 ± 0.030 (0.13 ± 0.030)	0.33 (0.33)	0.92 (0.92)	458
	Land	−0.03 ± 0.030 (−0.03 ± 0.030)	0.42 (0.42)	0.87 (0.88)	740	−0.06 ± 0.058 (−0.13 ± 0.057)	0.67 (0.66)	0.78 (0.79)	521	0.04 ± 0.024 (−0.07 ± 0.021)	0.40 (0.34)	0.90 (0.92)	1061
Asc	Ocean	0.31 ± 0.035	0.39	0.91	436	0.03 ± 0.024	0.30	0.12	98	−0.03 ± 0.022	0.30	0.13	718
	Land	–	–	–	–	–	–	–	–	–	–	–	–
Dar	Ocean	0.06 ± 0.041	0.38	0.92	337	0.01 ± 0.059	0.30	0.94	101	−0.15 ± 0.025	0.31	0.95	614
	Land	0.26 ± 0.019	0.37	0.89	1519	−0.02 ± 0.014	0.41	0.86	3103	0.06 ± 0.013	0.34	0.91	2774
Reu	Ocean	0.47 ± 0.033	0.36	0.84	467	−0.03 ± 0.056	0.35	0.83	153	−0.03 ± 0.019	0.27	0.87	766
	Land	0.24 ± 0.030	0.33	0.81	477	−0.20 ± 0.055	0.56	0.62	402	0.05 ± 0.025	0.30	0.82	542
Wol	Ocean	0.49 ± 0.046	0.41	0.81	302	−0.08 ± 0.058	0.38	0.92	162	0.01 ± 0.026	0.31	0.92	520
	Land	0.08 ± 0.022	0.53	0.82	2339	−0.03 ± 0.026	0.52	0.82	2513	0.00 ± 0.014	0.40	0.88	3026
All	Ocean	0.33 ± 0.018	0.41	0.89	1939	−0.03 ± 0.026	0.35	0.92	719	−0.06 ± 0.011	0.31	0.93	3076
	Land	0.13 ± 0.013	0.47	0.85	5075	−0.04 ± 0.012	0.49	0.84	6539	0.03 ± 0.008	0.37	0.90	7403

Table 4. XCH_4 results of NIES, SRFP and SRPR algorithms at 5 TCCON stations based on all individual TCCON-satellite data pairs. The 95 % confidence interval of relative bias, relative scatter, *R* and *N* are defined in Sect. 3.4. Between brackets are the results without altitude correction.

Site	Target	NIES_XCH$_4$				SRFP_XCH$_4$				SRPR_XCH$_4$			
		95 % Bias	Scatter	*R*	*N*	95 % Bias	Scatter	*R*	*N*	95 % Bias	Scatter	*R*	*N*
Iza	Ocean	0.19 ± 0.074 (−0.88 ± 0.075)	0.62 (0.63)	0.62 (0.62)	397	0.33 ± 0.061 (−0.89 ± 0.062)	0.64 (0.68)	0.59 (0.52)	180	0.16 ± 0.056 (−1.04 ± 0.055)	0.72 (0.70)	0.51 (0.48)	632
	Land	0.32 ± 0.054 (−0.63 ± 0.055)	0.64 (0.69)	0.72 (0.67)	740	−0.22 ± 0.046 (−1.30 ± 0.050)	0.92 (0.87)	0.53 (0.51)	521	−0.16 ± 0.025 (−1.10 ± 0.024)	0.64 (0.61)	0.68 (0.68)	2583
Asc	Ocean	−0.13 ± 0.063	0.73	−0.13	436	0.09 ± 0.069	0.51	−0.06	94	0.19 ± 0.070	0.98	−0.19	755
	Land	–	–	–	–	–	–	–	–	–	–	–	–
Dar	Ocean	−0.59 ± 0.069	0.65	0.62	337	−0.59 ± 0.130	0.56	0.57	73	−0.30 ± 0.055	0.69	0.53	600
	Land	0.38 ± 0.026	0.52	0.56	1519	−0.21 ± 0.021	0.61	0.43	3103	−0.04 ± 0.016	0.59	0.49	5494
Reu	Ocean	0.00 ± 0.048	0.53	0.58	467	−0.42 ± 0.084	0.47	0.70	120	−0.22 ± 0.045	0.62	0.39	720
	Land	−0.01 ± 0.046	0.51	0.41	477	−0.80 ± 0.066	0.67	0.31	402	−0.50 ± 0.044	0.67	0.17	907
Wol	Ocean	0.47 ± 0.070	0.62	0.58	302	0.03 ± 0.093	0.58	0.68	151	0.35 ± 0.079	0.83	0.37	416
	Land	0.42 ± 0.033	0.81	0.55	2339	−0.08 ± 0.032	0.81	0.56	2513	0.06 ± 0.023	0.80	0.56	4688
All	Ocean	−0.02 ± 0.032	0.71	0.87	1939	−0.04 ± 0.051	0.65	0.87	618	0.02 ± 0.028	0.81	0.80	3123
	Land	0.35 ± 0.019	0.69	0.81	5075	−0.20 ± 0.018	0.74	0.76	6539	−0.06 ± 0.012	0.70	0.81	13 672

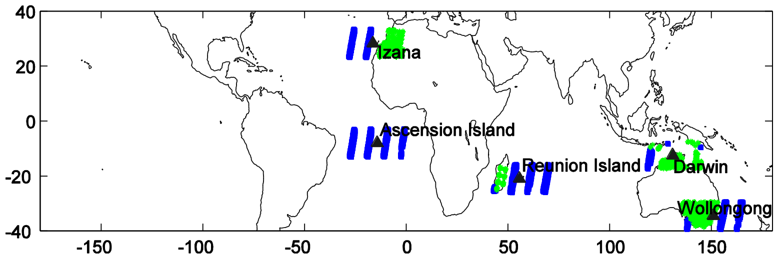

Figure 1. TCCON stations and SRPR XCH_4 co-located footprints from April 2009 to December 2013. The colocation box is chosen as ±5° latitude ±15° longitude around the TCCON station. The blue footprints are sun glint data over ocean and the green ones are data above land.

Discussion Paper | Discussion Paper | Discussion Paper | Discussion Paper |

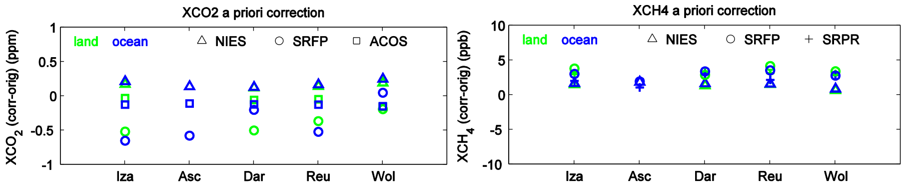

Figure 2. The average of the differences between a-priori-corrected and original satellite XCO_2 and XCH_4 retrievals (corrected – original) at five TCCON stations. Iza, Asc, Dar, Reu and Wol stand for Izaña, Ascension Island, Darwin, Reunion Island and Wollongong. The blue footprints are sun glint data over ocean and the green ones are data above land.

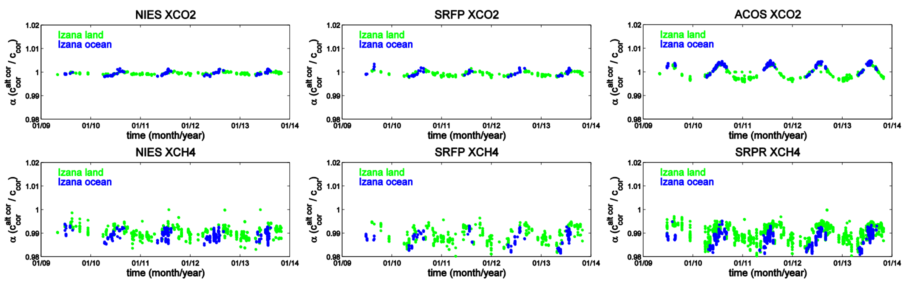

Figure 3. The time series plots of XCO_2 and XCH_4 altitude-correction factors for different GOSAT algorithms at the Izaña site. Blue data points are sun glint data over ocean and the green ones are data above land.

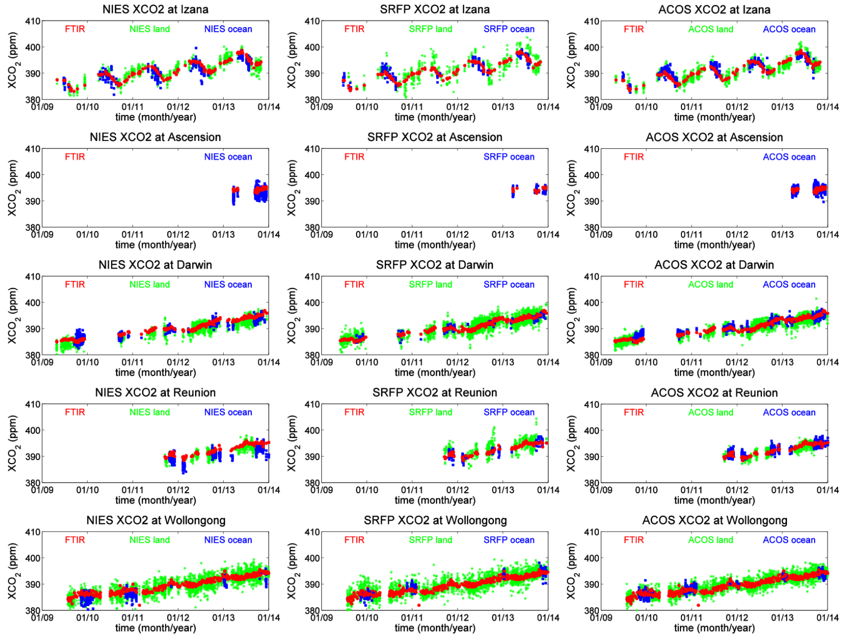

Figure 4. Time series plots of TCCON and GOSAT XCO_2 measurements based on the individual data pair. Left, middle and right panels correspond to NIES, SRFP and ACOS algorithms, respectively. Red points represent the FTIR measurements; blue and green ones represent the GOSAT glint data over ocean and the normal nadir data above land, respectively.

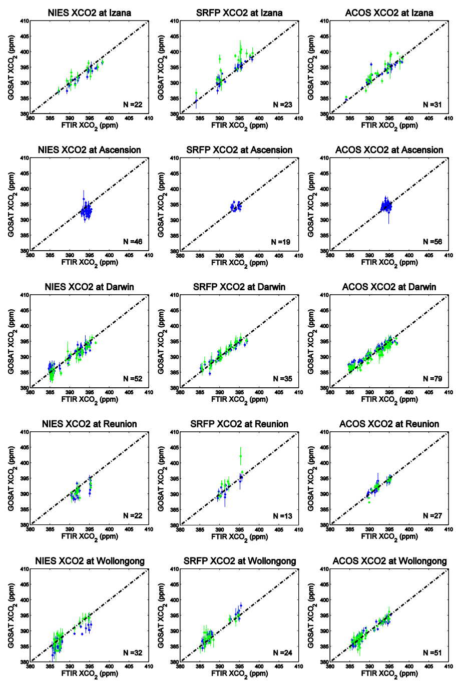

Figure 5. The scatter plots of daily median of XCO_2 from FTIR measurements and different GOSAT algorithms retrievals over 5 TCCON sites. Only the ocean and land data co-existing within ±1 day are selected; N is the total number of days. The error bar represents the standard deviation of all the measurements within ±1 day. The blue and green points present the glint mode over ocean and the normal nadir mode above land, respectively.

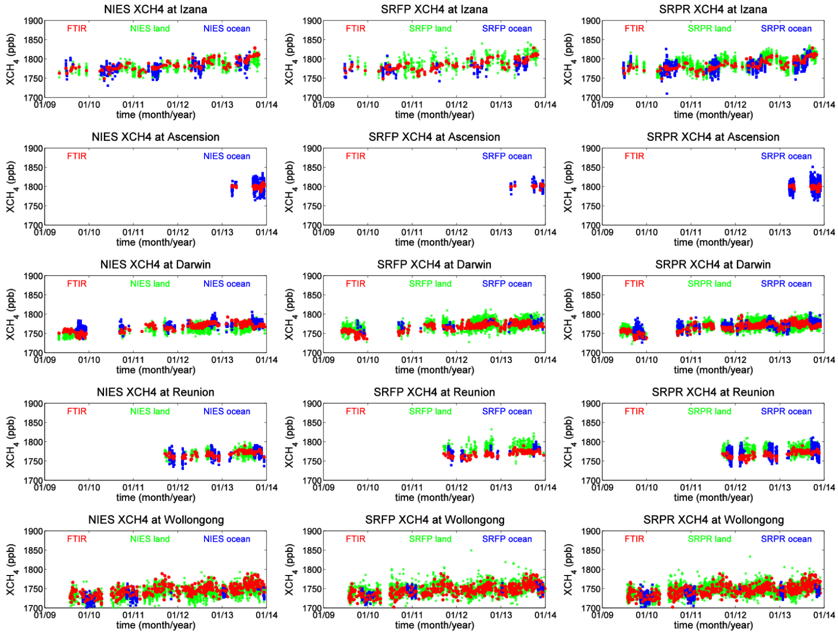

Figure 6. Time series plots of TCCON and GOSAT XCH_4 measurements based on the individual data pair. Left, middle and right panels correspond to NIES, SRFP and SRPR algorithms, respectively. Red, blue and green points represent the FTIR measurements, the GOSAT glint data over ocean and the normal nadir data above land, respectively.

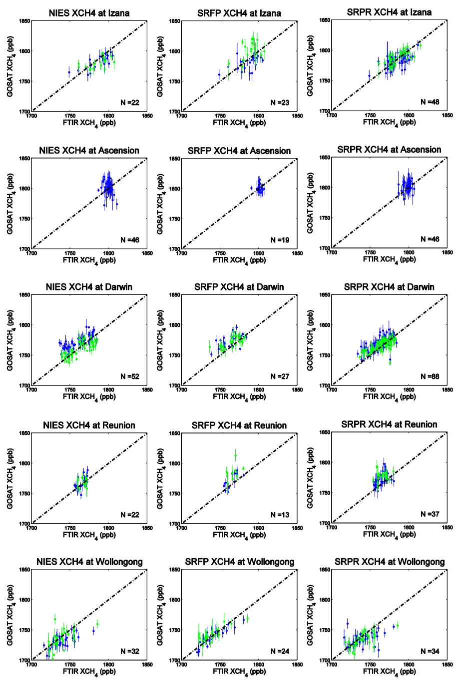

Figure 7. The scatter plots of daily median of XCH_4 from FTIR measurements and different GOSAT algorithms retrievals over 5 TCCON sites. Only the ocean and land data co-existing within ±1 day are selected; *N* is the total number of days. The error bar represents the standard deviation of all the measurements within ±1 day. The blue and green points present the glint mode over ocean and the normal nadir mode above land, respectively.

Discussion Paper | Discussion Paper | Discussion Paper | Discussion Paper |

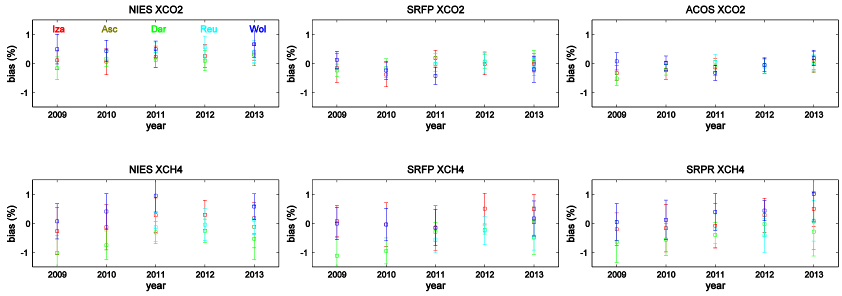

Figure 8. Annual mean bias of ocean data for each TCCON stations from different algorithms from 2009 to 2013. The error bar represents the standard deviation.